

To appear in the Proceedings of the 25th NSO Workshop

Evolution of Filament Barbs

Rui Liu, Yan Xu, & Haimin Wang

Space Weather Research Laboratory, Center for Solar-Terrestrial Research, NJIT, Newark, NJ 07102, USA e-mail: rui.liu@njit.edu

Abstract. We present a selected few cases in which the sense of chirality of filament barbs changed within as short as hours. We investigate in detail a quiescent filament on 2003 September 10 and 11. Of its four barbs displaying such changes only one overlay a small polarity inversion line inside the EUV filament channel (EFC). No magnetic elements with magnitude above the noise level were detected at the endpoints of all barbs. In particular, a pair of barbs first approached toward and then departed from each other in $H\alpha$, with the barb endpoints migrating as far as $\sim 10''$. We conclude that the evolution of the barbs was driven by flux emergence and cancellation of small bipolar units at the EFC border.

Key words. Sun: filaments

1. Introduction

Barbs are lateral extensions from the filament spine and apparently terminate in the chromosphere. Similar to the spine, they are composed of parallel, thin threads (e.g., Lin et al. 2005a). The direction in which they extend from the spine reveals the *chirality* of the filament, which follows a similar hemispheric rule as other solar magnetic structures (Martin 1998). Martin and colleagues (Martin & Echols 1994; Martin & McAllister 1997) have established empirically that a *dextral* (*sinistral*) filament has right-bearing (left-bearing) barbs in the same sense as right-hand (left-hand) ramps off an elevated highway, as which the filament spine is regarded by an analogy.

Martin & Echols (1994) suggested that the ends of barbs are fixed at patches of parasitic polarities (also termed minority polarities), which are opposite in polarity to the surrounding network elements. Contradictory

observations, however, have since been reported on this particular issue. For example, van Ballegoijen (2004) studied a barb terminated between the network elements, where the field is very weak, with no evidence for flux cancellation. Chae et al. (2005) reported that two barbs of an $H\alpha$ filament terminated over minority-polarity inversion lines. Lin et al. (2005a,b) found that the majority of barbs of quiescent filaments end within the network boundaries as represented by flow converging regions, where the fields are often too weak to be detected.

Two different 3D models have been proposed on how barbs are magnetically structured. Via morphological deductions, Martin and colleagues construct an *arcade model* (Martin & Echols 1994; Martin & McAllister 1997), in which both the spine and the barbs are composed of magnetic arcades aligned with thin threads, implying that barbs terminate in the parasitic polarity.

Alternatively, Aulanier and colleagues (Aulanier & Démoulin 1998; Aulanier et al.

Send offprint requests to: R. Liu

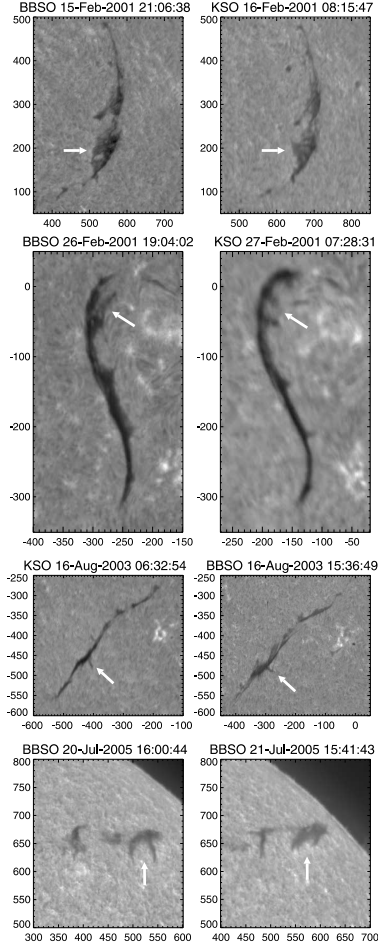


Fig. 1. Four events showing the orientation change of filament barbs, as marked by arrows. From top to bottom, the time difference between the left- and the right-column image are about 11, 12, 9, and 24 hours, respectively.

1998, 1999, 2000) model the $H\alpha$ absorbing features in the filament channel, i.e., the spine, the barbs, and the surrounding fibrils, as the dipped portions of field lines (hence named *dip model*). The dips in the barbs are formed by the perturbations of the background field due to the existence of parasitic polarities. With projection effects, a continuous pattern of dipped field lines could give the illusion that barbs are made of vertical fields joining the spine to the photosphere. The barb orientation

(i.e., right- or left-bearing), is not only constrained by the sign of magnetic helicity, but also by the distribution of parasitic polarities (Aulanier et al. 1999, 2000), whose evolution drives the evolution of barbs (Aulanier et al. 1999). Aulanier et al. (1998) showed that current dissipation at quasi-separatrix layers are associated with these lateral dips, where Ca II (8542 Å) brightenings were observed. Using magnetograms as boundary conditions, the filament structures were successfully reconstructed through a constant- α magnetohydrostatic extrapolation (Aulanier et al. 1999, 2000). The dip model has been further developed using non-linear force-free solutions (e.g., van Ballegoijen 2004).

Observation and modeling have been advanced to EUV, in which a filament is observed as a much wider intensity-depletion region than its $H\alpha$ counterpart (Heinzel et al. 2001). Wang (2001) reported that He II (304 Å) filaments are rooted in areas of on-going flux cancellation, and that those legs and barbs decay away after the cancellation. Aulanier & Schmieder (2002) found that the EUV filament channel (EFC) is dominated by extensions with similar morphology to $H\alpha$ barbs. In their data-driven modeling, $H\alpha$ structures are matched by high-altitude dips while the EFC by low-altitude ones. They identified the endpoints of $H\alpha$ barbs with weak parasitic polarities (3–10 G), while magnetic concentrations, shown as isolated bright patches in EUV, are at the outer parts of the EFC.

In this paper, we present observations of the dynamic evolution of filament barbs (Section 2), in which the sense of chirality, as defined in Martin (1998), can be changed within 24 hours. Concluding remarks are made in Section 3.

2. Observation and Analysis

From daily $H\alpha$ images obtained by Kanzelhöhe Solar Observatory (KSO) and Big Bear Solar Observatory (BBSO), a selected few examples are shown in Fig. 1, in which remarkable changes of the barb orientation occurred within 9–24 hours, which cannot be explained by the the change of perspective

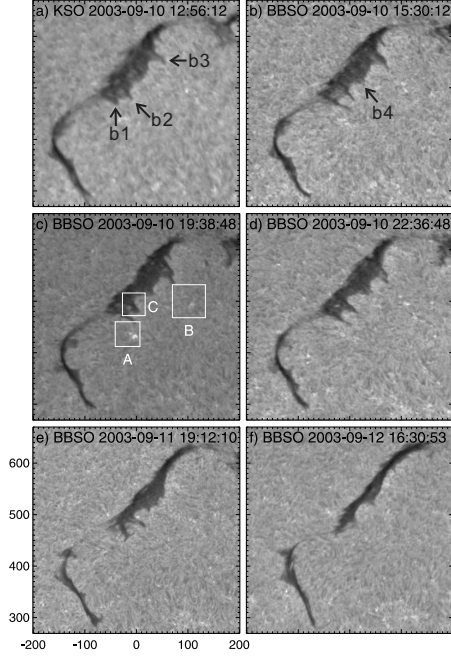


Fig. 2. Snapshots of KSO and BBSO $H\alpha$ images on 2003 September 10 and 11.

only. The first three cases show that the barbs marked by arrows changed from left to right-bearing, or vice versa. The last one shows that two barbs changed from apparently perpendicular to the spine to left-bearing.

Below we investigated in detail a quiescent filament in the northern hemisphere during 2003 September 10 and 11. In Fig. 2, snapshots of $H\alpha$ images show the highly dynamic and complicated evolution of the filament barbs. All images are registered to the one in Panel (e), in which the barbs were close to the disk center. In Fig. 2(a), marked by arrows are three barbs apparently perpendicular to the spine. As time progressed, $b1$ and $b2$ extended their lengths, and developed into a right-bearing and a left-bearing barb, respectively (Fig. 2(b)). Meanwhile, a new barb, $b4$, was forming to the southeast of $b3$ (Fig. 2(b)), while $b1$ began to “rotate” clockwise and $b2$ counterclockwise. As of 2003 September 11 19:12 UT (Fig. 2(e)), $b1$ has changed from right-bearing to left-bearing, opposite to the evolution of $b2$, while both $b3$ and $b4$ have

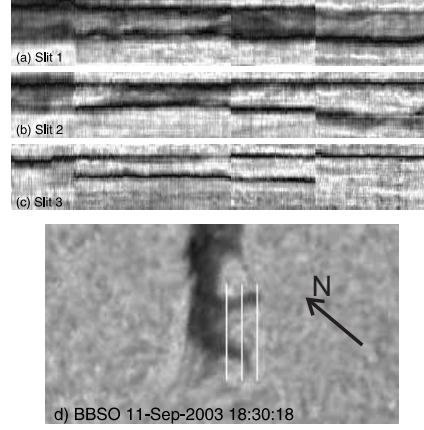


Fig. 3. $H\alpha$ slit images. Slits 1, 2, and 3 are positioned from left to right, respectively, as shown in the bottom panel. The arrow points to the north.

developed into left-bearing barbs. On the next day (2003 September 12), all four barbs almost disappeared (Fig. 2(i)).

Particularly interesting is the evolution of $b1$ and $b2$. In Fig. 3(d), they are rotated to a “horizontal” position. Before that, we have aligned and then de-stretched $H\alpha$ images to correct image jitter and warping. We then put three slits across $b1$ and $b2$ (Fig. 3(d)), referred to as Slits 1, 2, and 3, from left to right, respectively. Slices of $H\alpha$ images cut by the slits are shown in Fig. 3(a)–(c), in which $b1$ (lower streak) and $b2$ (upper streak) first approached toward, and then departed from, each other, during the two-day interval. Note that the discontinuities are due to data gaps (see also Fig. 5).

Two $H\alpha$ brightening regions nearby the barbs of interest are identified in Fig. 2(d) (labelled A and B), with corresponding brightening in SOHO/EIT 195 Å (see Fig. 4). When overlaying the $H\alpha$ filament and SOHO/MDI magnetograms on corresponding EIT 195 Å images (Fig. 4), one can see that both brightening regions are co-spatial with dipolar units composed of a magnetic element of parasitic (negative) polarity in close contact with magnetic element(s) of major (positive) polarity. A third dipolar unit which is spatially associated with $b2$ is denoted as C (Fig. 2(d) and Fig. 4).

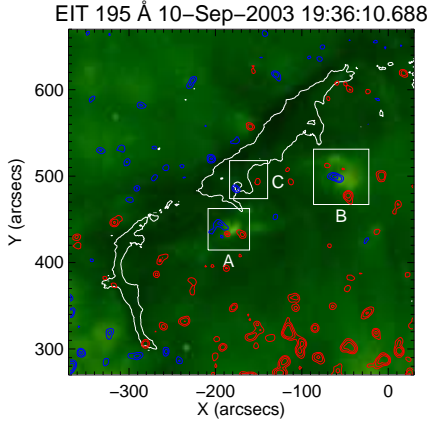


Fig. 4. EIT 195 Å image overlaid by $H\alpha$ filament (white contours) and MDI magnetogram. Contour levels of fields are 30, 60, and 120 G for positive polarities (red), and -120, -60, and -30 G for negative polarities (blue).

Integrating MDI flux over the three rectangular regions, inside which the dipolar units are localized over the two-day interval, one can see that significant flux emergence and cancellation of minor polarity occur in both Regions A and B, while there is minimal activity in Region C (Fig. 5(b) and (c)). Interestingly, the profile of MDI fluxes bears a remarkable similarity to that of EIT data counts in the same region (Fig. 5), suggestive of the connection of the two phenomena.

3. Conclusion

Of the four barbs displaying obvious changes of orientation on 2003 September 10 and 11, *b2* is the only one overlying a small polarity inversion line inside the EFC (Fig. 4). The endpoints of the rest three barbs are not fixed at any magnetic element with magnitude above the noise level. It is unlikely that changes of such weak fields would result in the “migration” of the barb ends as far as $\sim 10''$ (see Fig. 5(a)). It is more intuitive, however, to conclude that the barbs are not rooted in the photosphere, but their evolution was associated with flux emergence and cancellation of the dipole units at the EFC border. This casts doubt on the

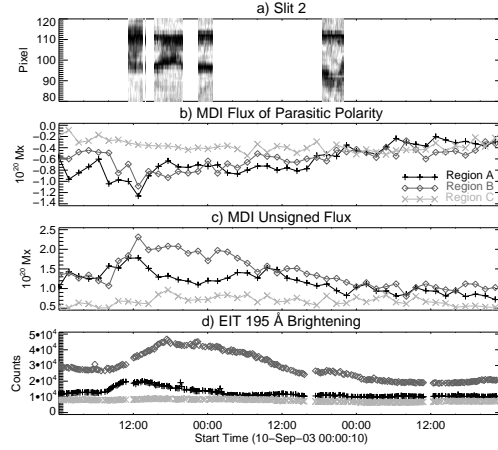


Fig. 5. Profiles of MDI fluxes and EIT 195 Å data counts integrating over the regions specified in Fig. 4, along with slices of $H\alpha$ images cut by Slit 2.

reliability of barbs as the indicator of the filament chirality.

Acknowledgements. $H\alpha$ data are provided through the Global High Resolution H-alpha Network. This work was supported by NASA grant NNX08-AJ23G and NNX08-AQ90G, and by NSF grant ATM-0849453 and ATM-0839216.

References

- Aulanier, G. & Démoulin, P. 1998, *A&A*, 329, 1125
- Aulanier, G., et al. 1999, *A&A*, 342, 867
- Aulanier, G., et al. 1998, *A&A*, 335, 309
- Aulanier, G. & Schmieder, B. 2002, *A&A*, 386, 1106
- Aulanier, G., et al. 2000, *ApJ*, 543, 447
- Chae, J., et al. 2005, *ApJ*, 626, 574
- Heinzel, P., et al. 2001, *ApJ*, 561, L223
- Lin, Y., et al. 2005a, *Sol. Phys.*, 226, 239
- Lin, Y., et al. 2005b, *Sol. Phys.*, 227, 283
- Martin, S. F. 1998, *Sol. Phys.*, 182, 107
- Martin, S. F. & Echols, C. R. 1994, in *Solar Surface Magnetism*, ed. R. J. Rutten & C. J. Schrijver, 339
- Martin, S. F. & McAllister, A. H. 1997, in *Coronal Mass Ejections*, ed. N. Crooker et al., *Geophysical Monograph* 99, 127
- van Ballegoijen, A. A. 2004, *ApJ*, 612, 519
- Wang, Y.-M. 2001, *ApJ*, 560, 456